Research paper

Net section resistance of steel angles connected by one leg

Edyta Bernatowska[1], Lucjan Ślęczka[2]

Abstract: In civil engineering structures, steel angles are often used as tensioned elements, because of their ease of fabrication and assembly. For practical reasons, angles are usually connected only by one leg, using a single row of bolts, and rupture of weakened section usually determines a joint capacity. Also, eccentricity affects the distribution of stresses in the net section and hence its load capacity. Assessment of ultimate resistance is a completely different issue compared to the well-known and established problems of plastic resistance and requires advanced material modelling. The paper presents a numerical simulation of net section failure of tensioned angles, made of structural steel grade S275, taking into account ductile initiation and propagation of fracture using the Gurson–Tvergaard–Needleman damage model. Extensive parametrical analysis of ultimate tensile resistance was performed with a wide range of parameters. The typical and well-recognised failure modes were observed as net section fracture and block tearing. Also, an additional failure mode, classified as limited block tearing, has occurred which is not considered in current design provisions. The paper describes the impact of individual geometrical properties of the joint (numbers of bolts, connection length, and distance from the edge of the connected leg to the center of the fastener hole) on the apparent failure form and the resistance obtained.

Keywords: lap-bolted connection, steel angles, net section fracture, block tearing, numerical simulations

[1]PhD., Eng., Rzeszów University of Technology, Faculty of Civil and Environmental Engineering and Architecture, Poznańska 2, 35-084 Rzeszów, Poland, e-mail: e_bernat@prz.edu.pl, ORCID: 0000-0003-0591-5202
[2]DSc., PhD., Eng., Rzeszów University of Technology, Faculty of Civil and Environmental Engineering and Architecture, Poznańska 2, 35-084 Rzeszów, Poland, e-mail: sleczka@prz.edu.pl, ORCID: 0000-0002-8979-7073

1. Introduction

Steel angles are often used as tensioned elements in building structures, especially as bracings. The most common form of their joining, resulting from the cross section shape, is connecting of the angle profile by only one leg, while the other outstanding leg remains unconnected. If bolts are used as fasteners, the cross section of the connected leg is additionally weakened. Both of these influences (the weakening of the cross section and the effect of eccentricity) cause an uneven stress distribution in connected angle.

During the design of such elements, in addition to considering the plastic resistance of the gross cross section, the ultimate resistance of the net cross section and block tearing resistance should also be taken into account. The ultimate resistance of the net cross section perpendicular to the direction of load transfer A_{net} is based on material rupture (Fig. 1a). Block tearing is considered as a limit state that combines shear failure at the line of bolts along the shear face of the bolt hole group and tensile rupture along the line of bolt holes on the tension face of the bolt group, as shown in Fig. 1b. As can be seen, steel rupture affects these two failure modes and the precise prediction of ductile fracture under complex stress states becomes important in the prediction of the ultimate resistance of such joints.
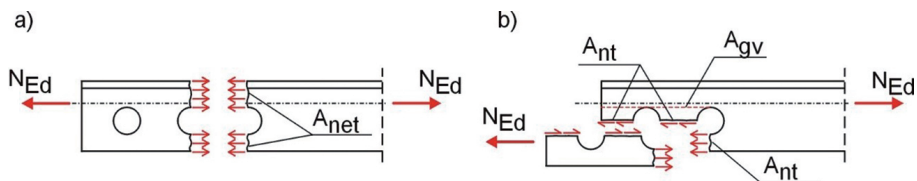

Fig. 1. Failure modes of angles connected by one leg considered in design provisions:
a) rupture of net cross section, b) block tearing

Many researchers carried out extensive experimental studies on single or double angle tension members, e.g. [1–5], which led to the proposition of phenomenological strength functions based on simple engineering models. Finite element studies of ultimate joint resistance are much rarer and were often performed with a relatively high degree of simplification [1, 6, 7]. In some of them angles were modelled with shell elements, and in others important parts, like bolts, were omitted. A fracture strain criterion and a traditional elastoplastic hardening model were often used to simulate the ultimate state of tensioned joints, but this approach may overestimate the localization effect of plasticity in the necking zone, if material damage is not considered [8].

Today, more sophisticated FE techniques are used to simulate ductile damage to elements and connections [9]. They can reproduce both net cross-section rupture and block tearing [3, 10, 11] but so far there is a lack of a larger parametric analysis of the ultimate resistance angles connected by one leg. Also, during such analysis, emphasis should be placed not only on the global connection behaviour and the resulting load capacity, but also on local effects and appearing failure modes.

This paper relates to steel angle tension members connected by one row of bolts and to the prediction of their ultimate resistance by means of FEA. The Gurson–Tvergaard–

Needleman (GTN) material model was applied to simulate the material failure process. It is a micromechanics-based porous plasticity model considering the effect of void growth and coalescence. It was proposed by Gurson [12], later modified by Tvergaard and Needleman [13] and is now widely used in modelling of damage and fracture simulation of steel structures [8, 14–16].

The main part of the paper consists of a parametric analysis taking into account the influence of geometric and material parameters on the ultimate resistance of angles connected by one leg and the observed failure mode.

2. Finite element modelling

2.1. General approach

Finite element models consisted of four components: angle, gusset plate, bolt with nut, and washers. Due to symmetry and to save calculation time, only half of the angle specimens were modelled. For angle, gusset plates and washers three-dimensional, hexahedral 8-node linear brick with reduced integration C3D8R was used from ABAQUS software library. This type of element has been shown to be suitable for simulating lap-bolted connections [7, 17]. Bolts were built using C3D8T and C3D6T elements, which are, respectively, 8-node thermally coupled bricks with trilinear displacement and temperature and 6-node thermally coupled triangular prism used to complete the mesh. To apply a small clamping force starting from snug-tightened bolts, the vertical thermal deformation method was utilized [18]. Contact between surfaces was defined using the general contact option. The frictional effects between surfaces were also included by incorporating the classical isotropic Coulomb friction model in the definition of contact, with a friction coefficient μ equal to 0.1. No imperfections were included in the model, neither geometric nor material. Especially the ideal bolt alignment was considered – initially, before applying a load, both washers and bolts were located concentrically with holes in the angle and the gusset plate. The picture below (Fig. 2) presents the view on the complete model. All models were developed using the ABAQUS package. The Gurson-Tvergaard-Needelman (GTN) material model was applied to influence material rupture (see the next paragraph), and for this reason FE modelling required dynamic explicit analysis.
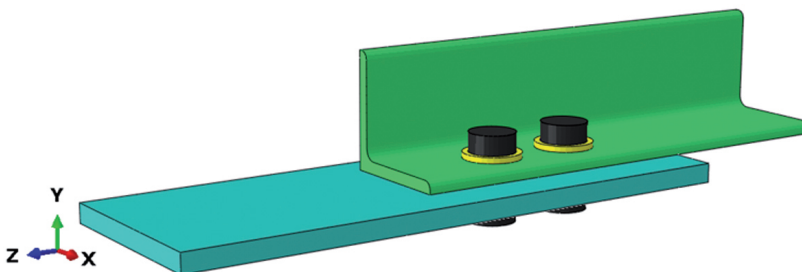

Fig. 2. Example model of an angle specimen

2.2. Material modelling

The properties of the chosen material were based on relevant material tests, from the experimental study conducted [19]. The mean value of the yield stress f_y was 288 MPa, and the mean value of the ultimate stress f_u was 425 MPa, so such properties conformed to the steel grade S275.

To take into account the influence of microstructural damage on load capacity and material strength, the Gurson-Tvergaard-Needelman (GTN) material model was implemented. This type of material, is classified as porous material where damage of the microstructure occurs in the form of voids, which are initiated on the inclusions present in the material. The destruction process takes place through the growth and merging of voids through localized plastic deformation. This model is intended for use in fracture or damage analysis, and its purpose is to predict ductile crack behaviour through void growth and coalescence [12]. The GTN failure criterion is expressed as follows:

$$(2.1) \qquad \Phi = \left(\frac{\sigma_e}{\sigma_y}\right)^2 + 2q_1 f^* \cosh\left(q_2 \frac{3\sigma_m}{2\sigma_y}\right) - \left(1 + q_3 f^{*2}\right) = 0$$

where: Φ – non-dilatational strain energy, σ_e – effective stress according to the Huber-Mises-Hencky hypothesis, σ_y – yield stress of the material, σ_m – hydrostatic pressure (mean stress), f^* – modified void volume fraction, q_i – Tvergaard's parameters describing the plastic properties of the material. Typical values of these parameters are: $q_1 = 1.5$; $q_2 = 1.0$ and $q_3 = q_1^2 = 2.25$.

The modified void volume fraction f^* is defined as follows:

$$(2.2) \qquad f^* = \begin{cases} f & \text{for } f \leq f_c \\ f_c + \dfrac{\overline{f}_F - f_c}{f_F - f_c}(f - f_c) & \text{for } f_c < f < f_F \\ \overline{f}_F & \text{for } f \geq f_F \end{cases}$$

where: f – current volume fraction of the void, f_c – critical volume fraction of the coalescence of the void at which the void coalescence starts, f_F – volume fraction of the void corresponding to the complete loss of material strength, at the final separation of the material $\overline{f}_F = \left(q_1 + \sqrt{q_1^2 - q_3}\right)/q_3$.

When the material is not subjected to loading and deformation, the modified void volume fraction f^* is equal to the initial void volume fraction f_0, which is a basic GTN material parameter connected to the porosity of the material. The value of this parameter can be calculated based on the chemical composition, where Mn and S are the percentages of manganese and sulphur inclusions determined from the chemical composition of steel, based on nominal values from [20], or on microstructural tests:

$$(2.3) \qquad f_0 = 0.54\left(S\% - \frac{0.001}{Mn\%}\right)$$

Critical void volume fraction f_c occurs when the load capacity of the element decreases. It is related to the value f_0, but it can also be determined by matching the σ–ε curve

obtained from numerical simulations with that obtained from experimental tests. The f_F value corresponds to the destruction of the material and for metals ranges from 0.10 to 0.20. It can also be determined experimentally [21, 22].

The evolution of damage is described by the parameters f_N, ε_N and s_N. The first parameter defines the volume fraction of nucleated voids, which for structural steels can be assumed to be 0.04. The deformation level that creates new voids is described by the ε_N. A typical value for steel is $\varepsilon_N = 0.30$. The normal distribution of the nucleation strain of the voids is determined by the standard deviation s_N assumed in the range of 0.01 to 0.10.

Hierarchical validation of computational models based on own experimental data was described in [23, 24]. Very good accuracy was observed in the failure load predictions. The final material parameters that were introduced into the ABAQUS program are presented in Table 1.

Table 1. GTN material model parameters

f_0	q_i	f_N	ε_N	s_N	f_c	f_F
0.001	$q_1 = 1.5$; $q_2 = 1.5$; $q_3 = 1.5$	0.02	0.3	0.1	0.06	0.2

3. Parametric analysis

3.1. General description of parametric analysis models

To determine the impact of individual geometric parameters on the global behaviour of the joints and their tensile resistance, parametric analysis was carried out. Eighty-eight numerical models were built, divided into eight groups, where the following parameters were investigated:

– the ratio of the width of the leg to its thickness b/t (slenderness of the angle walls), in equal leg angles (A1),
– the spacing between the centres of the fasteners in a line in the direction of load transfer p_1 and the total length of the connection L_p (A2),
– the edge distance from the centre of a fastener hole to the adjacent edge of the angle, measured at right angles to the direction of load transfer e_2 (A3),
– the end distance from the center of a fastener hole to the adjacent end of the angle, measured in the direction of load transfer e_1 (A4),
– profile arrangement in connection: joining with a wider or narrower leg in the case of unequal angles (A5),
– angle length (A6),
– profile doubling: single angles vs. double angles (A7),
– differentiation of mechanical parameters of steel: elongation and proportion of f_u/f_y (A8).

In this paper only the results obtained in groups A1÷A4 and A8 are discussed. Figure 3 presents the model scheme with main dimensions and boundary conditions.
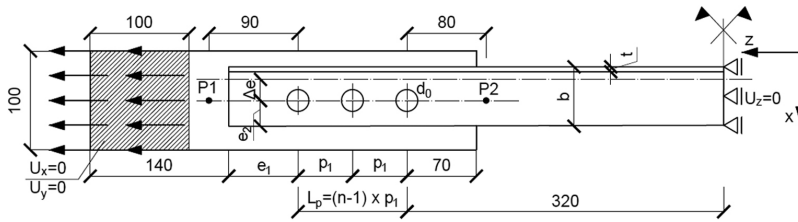
Fig. 3. Geometry of the bolted angle numerical model

The thickness of the gusset plate was equal to 10 mm except group A7 with double angles, where in some cases it was increased to avoid the failure of gusset plate. Points P1 and P2 were used to determine the longitudinal displacement. The number of bolts varied from $n = 1$ to $n = 5$. The diameters of the bolts used were M18 and M20, respectively, for connection with one and more than one bolt. The diameter of the bolt hole was 2 mm larger than the diameter of the bolt. Connection models were created in such a way as to cause only the failure of the angle member (it was the weakest component). The resistances of the bolts and the gusset plate were greater than the expected tensile resistance of the angle member.

The analysis took into account the sizes of angles produced in the steel mills, as well as several cross sections created only for the purpose of analysis to obtain extreme geometrical proportions of both the cross section and the connection. Due to this, "model similarity" was achieved to the entire population of angle profiles of various sizes, connected with bolts with different diameters.

3.2. Results obtained from simulations

The results obtained from the analyses were as follows:

– Force-displacement curves $F - \Delta$ for each analysed connection, where F is transmitted force and Δ is difference in longitudinal displacements of points P1 and P2 (Fig. 4).
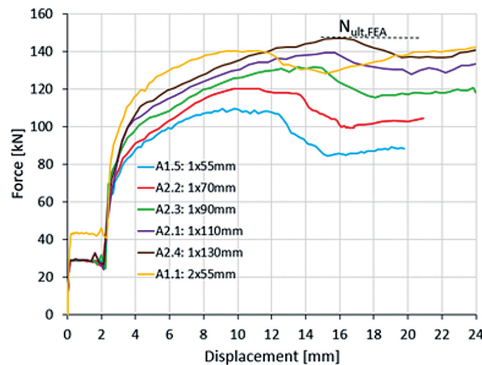

Fig. 4. Force displacement curves from group A2 for $L60 \times 6$ angles

- The tensile resistance (failure load) $N_{ult,FEA}$ obtained as the maximum force reached during loading history, from the force-displacement curve $F - \Delta$.
- Net cross-section efficiency factor U_{eff}, calculated from formula:

$$(3.1) \qquad U_{eff} = \frac{N_{ult,FEA}}{(A_{net} \cdot f_u)}.$$

- Distribution of effective stresses σ_{eff} (according to the Huber-Mises-Hencky hypothesis) for the failure load $N_{ult,FEA}$ in the section under block tearing along two paths (one is the net area subjected to shear, the second is the gross area subjected to shear). Their definitions are presented in Fig. 5a. In the same figure, the distribution of effective stresses σ_{eff} along the net section with the net shear area, for failure load $N_{ult,FEA}$, characterizing different failure modes is shown (Fig. 5a–5d).
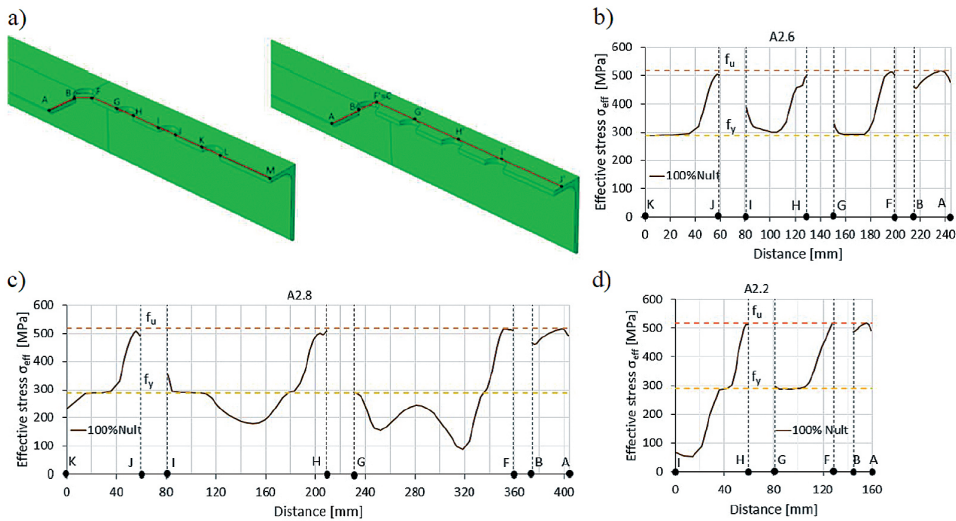

Fig. 5. Section subjected to block tearing and effective stress distribution: a) path definition (net area subjected to shear and gross area subjected to shear), b) effective stress distribution for block tearing (BT), c) for net section tearing failure mode (NT), d) for limited block tearing failure mode (BT-L)

- Form of the angle failure. During analyses three failure modes were distinguished: block tearing (further in the text marked with the symbol BT), net section tearing (symbol NT) and limited block tearing failure mode (BT-L). The main premise for determining the failure mode was the effective stress σ_{eff} distribution observed for the failure load level $N_{ult,FEA}$ on the face of the angle section (Fig. 6) and along the above defined paths.

Elements where the effective stresses σ_{eff} along the F–M (or F′J′) line achieved or exceeded the value f_y were classified as subjected to the block tearing failure mode (Fig. 5b and 6a). If stresses throughout this path (between bolt holes) did not reach the yield point, the failure mode was recognized as net section tearing (Fig. 5c and 6b). When
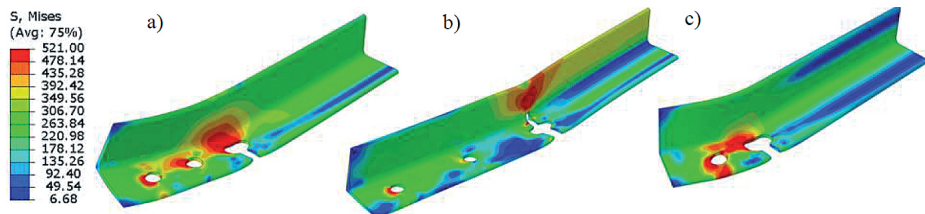
Fig. 6. Failure modes obtained: a) block tearing BT, b) net section tearing NT, c) limited block section tearing BT-L

effective stresses σ_{eff} did not reach f_y only in the region of end distance e_1, the element was classified as subject to the limited block tearing failure mode (Fig. 5d and 6c).

The latter failure mode (named here limited block tearing) turned out to be unusual and has not been distinguished so far in the design provisions. It consists of tensile rupture along the line of the first bolt hole on the tension face ($A_{nt,1}$ area), accompanied by plastic shear failure at the bolt hole line (A_{nv} area) and additional plastic failure at the perpendicular line from the last bolt hole ($A_{nt,2}$ area), see Fig. 7. The tear-out portion of the angle leg is limited, compared to typical block tearing failure (vide Fig. 1b).
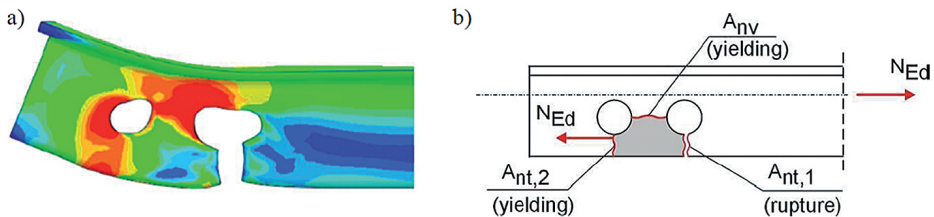

Fig. 7. Failure mode of limited block tearing: a) effective stress distribution observed in FEA, b) mechanism of limited block tearing

The rupture that appeared in FEA was always related to $A_{nt,1}$ section. The shear area was heavily stressed, but no fracture has been observed in this region, only yield bands have occurred (in block tearing failure), similar to $A_{nt,2}$ cross section in limited block tearing. All these failure modes were also obtained during experimental study and validation of FE models [19]. Angles connected by a single bolt were treated as separate cases, and their failure mode was not distinguished.

4. Results

4.1. Influence of the slenderness of the angle wall (*b/t*) – group A1

In the first group (A1), the purpose of the performed analyses was to check how the slenderness of the angle wall affects ultimate capacity and failure mode. This slenderness is described by the ratio of leg width to its thickness, b/t. Fifteen joints were tested, which

consisted of equal leg angles, with a b/t ratio ranging from 10 to 18. Their geometrical description is given in Table 2.

Table 2. List of elements analysed from group A1

Designation	Section	b/t	Bolt	Number of bolts, n	e_1 [mm]	e_2 [mm]	p_1 [mm]	$N_{\text{ult,FEA}}$ [kN]	U_{eff}	Failure mode
A1.1	$L60 \times 5$	12	M20	3	70	26	55	140.3	0.70	BT-L
A1.2	$L70 \times 5$	14	M20	3	70	33	55	164.4	0.67	BT-L
A1.3	$L80 \times 5$	16	M20	3	70	41	55	197.0	0.69	BT
A1.4	$L90 \times 5$	18	M20	3	70	48	55	221.9	0.67	BT
A1.5	$L60 \times 5$	12	M20	2	70	26	55	109.4	0.55	BT-L
A1.6	$L70 \times 5$	14	M20	2	70	33	55	132.6	0.54	BT-L
A1.7	$L75 \times 5$	15	M20	2	70	37	55	147.3	0.56	BT-L
A1.8	$L80 \times 5$	16	M20	2	70	41	55	160.0	0.56	BT-L
A1.9	$L50 \times 5$	10	M18	1	70	21	–	56.1	0.35	–
A1.10	$L60 \times 5$	12	M18	1	70	26	–	73.9	0.36	–
A1.11	$L65 \times 5$	13	M18	1	70	30	–	88.6	0.39	–
A1.12	$L70 \times 5$	14	M18	1	70	33	–	98.9	0.40	–
A1.13	$L70 \times 5.8$	12.1	M20	3	70	33	55	185.0	0.66	BT-L
A1.14	$L70 \times 5.8$	12.1	M20	2	70	33	55	152.2	0.54	BT-L
A1.15	$L70 \times 5.8$	12.1	M18	1	70	33	–	115.5	0.41	–

The results obtained in this group show negligible influence of the b/t ratio on the net section load capacity. Figure 8 shows the net efficiency factor for the cross section U_{eff} as a function of the b/t ratio. No form of failure by tearing the net cross section was obtained in any of the elements.
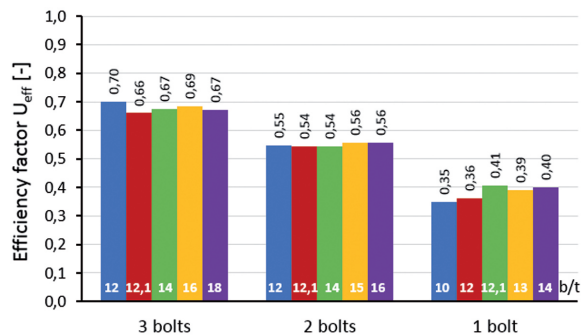

Fig. 8. Influence of b/t ratio on the net cross-sectional efficiency factor U_{eff}

4.2. Influence of the connection length – group A2

In group A2, the variable parameters were the number of bolts in connection n and their spacing p_1. To check their influence on the load capacity, 12 models were created and additionally 4 models from the A1 group were used. Table 3 presents a summary of these analyses. Figure 9 shows the influence of the relative length of the connection L_p/d_0

Table 3. List of elements analysed from group A2

| Designation	Section	Bolt	Number of bolts, n	e_1 [mm]	e_2 [mm]	p_1 [mm]	L_p [mm]	$N_{\text{ult,FEA}}$ [kN]	U_{eff}	Failure mode
A2.1	$L60 \times 5$	M20	2	70	26	110	110	139.5	0.70	NT
A2.2	$L60 \times 5$	M20	2	70	26	70	70	120.4	0.60	BT-L
A2.3	$L60 \times 5$	M20	2	70	26	90	90	131.7	0.66	BT-L
A2.4	$L60 \times 5$	M20	2	70	26	130	130	147.0	0.73	NT
A2.5	$L80 \times 5$	M20	2	70	41	110	110	195.3	0.68	NT
A2.6	$L80 \times 5$	M20	3	70	41	70	140	215.4	0.75	BT
A2.7	$L80 \times 5$	M20	3	70	41	95	190	232.1	0.81	NT
A2.8	$L80 \times 5$	M20	3	70	41	150	300	245.7	0.86	NT
A2.9	$L80 \times 5$	M20	4	70	41	50	150	214.3	0.75	BT
A2.10	$L80 \times 5$	M20	4	70	41	70	210	234.4	0.82	NT
A2.11	$L80 \times 5$	M20	4	70	41	90	270	241.8	0.84	NT
A2.12	$L80 \times 5$	M20	5	70	41	75	300	244.7	0.85	NT
A1.1	$L60 \times 5$	M20	3	70	26	55	110	140.3	0.70	BT-L
A1.3	$L80 \times 5$	M20	3	70	26	55	110	197.0	0.69	BT
A1.5	$L60 \times 5$	M20	2	70	41	55	55	109.4	0.55	BT-L
A1.8	$L80 \times 5$	M20	2	70	41	55	55	160.0	0.56	BT-L
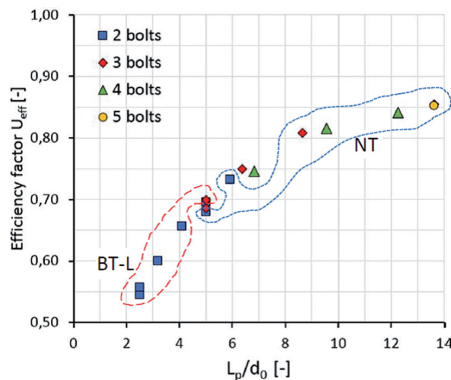
Fig. 9. Influence of relative connection length (L_p/d_0) on efficiency factor U_{eff}

(where d_0 is the diameter of the bolt hole) on the efficiency factor U_{eff} and also on the failure mode. As can be seen, the occurrence of net section tearing is characterized by significant U_{eff} values between 0.68 and 0.86. The points on the plot $L_P/d_0 - U_{\text{eff}}$ form a curve approaching a certain asymptote. The smallest values of the efficiency factor U_{eff} appear in the case of limited block tearing (BT-L).

4.3. Influence of distance e_2 – group A3

Group A3 was characterized by a variable value of the distance from the axis of the holes to the edge e_2 (measured in the direction perpendicular to the load direction), and thus the same distance from the axis of gravity of the section Δe (eccentricity of the tensile force, see Fig. 3). It was analysed how this parameter affects two sizes of angles ($L60 \times 5$ and $L80 \times 5$) with shorter and longer connection length (from 1 to 4 bolts in a joint). 13 new connections models were made, as well as 3 models from the A1 group were used. Their full description is provided in Table 4.

Table 4. List of elements analysed from group A3

Designation	Section	Bolt	Number of bolts, n	e_1 [mm]	e_2 [mm]	p_1 [mm]	Δe [mm]	$N_{\text{ult,FEA}}$ [kN]	U_{eff}	Failure mode
A3.1	$L60 \times 5$	M18	1	70	21	–	22.6	58.4	0.29	–
A3.2	$L60 \times 5$	M18	1	70	24	–	19.6	66.6	0.33	–
A3.3	$L60 \times 5$	M18	1	70	30	–	13.6	87.4	0.43	–
A3.4	$L80 \times 5$	M20	2	70	24	55	34.8	98.4	0.34	BT-L
A3.5	$L80 \times 5$	M20	2	70	30	55	28.8	118.4	0.41	BT-L
A3.6	$L80 \times 5$	M20	2	70	36	55	22.8	140.3	0.49	BT-L
A3.7	$L80 \times 5$	M20	2	70	46	55	12.8	183.7	0.64	BT
A3.8	$L80 \times 5$	M20	3	70	24	55	34.8	139.2	0.48	BT-L
A3.9	$L80 \times 5$	M20	3	70	36	55	22.8	177.6	0.62	BT-L
A3.10	$L80 \times 5$	M20	3	70	46	55	12.8	216.3	0.75	BT
A3.11	$L80 \times 5$	M20	4	70	24	55	34.8	163.4	0.57	BT-L
A3.12	$L80 \times 5$	M20	4	70	36	55	22.8	198.9	0.69	BT-L
A3.13	$L80 \times 5$	M20	4	70	46	55	12.8	238.8	0.83	BT
A1.3	$L80 \times 5$	M20	3	70	41	55	17.8	197.0	0.69	BT
A1.8	$L80 \times 5$	M20	2	70	41	55	17.8	160.0	0.56	BT-L
A1.10	$L60 \times 5$	M18	1	70	26	–	17.6	73.9	0.36	–

The relationship between relative eccentricity $\Delta e/b$ and the efficiency factor U_{eff} is shown in Fig. 10. An increase in the value of e_2 (and thus a decrease in Δe) causes an

increase in the load capacity of the net resistance, and an increase in the global ductility of the connection. Also increase of the value of e_2 influence on change in failure form, from limited block tearing into block tearing.
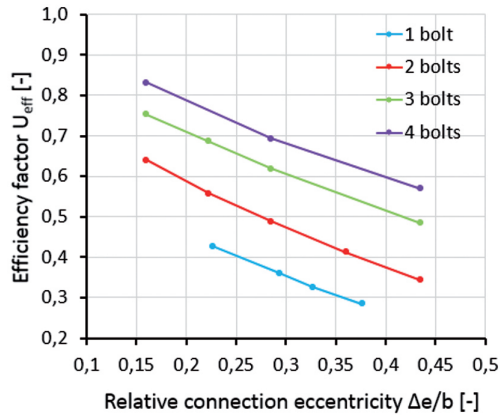

Fig. 10. Influence of relative connection eccentricity ($\Delta e/b$) on efficiency factor U_{eff}

4.4. Influence of end distance e_1 – group A4

In the next group, the only variable parameter was the end distance from the centre of a fastener hole to the adjacent end of the angle leg e_1, measured in the direction of load transfer. Nine models of connections with 1, 2, and 3 bolts were analysed. They were based on connections already analysed: A1.10 (with 1 bolt), A2.2 (2 bolts), and A2.6 (3 bolts), creating additional models with a shorter and longer e_1 distance (Table 5).

Table 5. List of elements analysed of group A4

Designation	Section	Bolt	Number of bolts, n	e_1 [mm]	e_2 [mm]	p_1 [mm]	$N_{\text{ult,FEA}}$ [kN]	U_{eff}	Failure mode
A4.1	$L60 \times 5$	M20	2	50	26	70	119.4	0.60	BT-L
A2.2	$L60 \times 5$	M20	2	70	26	70	120.4	0.60	BT-L
A4.2	$L60 \times 5$	M20	2	90	26	70	120.1	0.60	BT-L
A4.3	$L80 \times 5$	M20	3	30	41	70	211.5	0.74	BT
A4.4	$L80 \times 5$	M20	3	50	41	70	215.5	0.75	BT
A2.6	$L80 \times 5$	M20	3	70	41	70	215.4	0.75	BT
A4.5	$L80 \times 5$	M20	3	90	41	70	216.2	0.75	BT-L
A4.6	$L60 \times 5$	M18	1	90	26	–	73.8	0.36	–
A1.10	$L60 \times 5$	M18	1	70	26	–	73.9	0.36	–

In connections with only one bolt, the change in length e_1 does not affect the resistance of the net cross section. In connections with two or more bolts, it can be seen from the comparison of A4.3, A4.4, A2.6, and A4.5 that increasing the length e_1 can change the failure mode. With a smaller distance e_1, the connection is subjected to block tearing, with a larger distance e_1, failure occurs through limited block tearing. Later, this hypothesis will be checked on the basis of results of all modelled connections.

4.5. Influence of steel grade

In all the groups discussed above, the influence of geometrical parameters on the connection was analyzed. In the last group (A8), the influence of the mechanical parameters of the steel was considered. The yield strength, tensile strength and ductility values were changed, so the created material characteristics corresponded additionally to the grades: S235 (f_y = 235 MPa, f_u = 360 MPa) and S450 (f_y = 440 MPa, f_u = 550 MPa), Table 6.

Table 6. List of elements analysed from group A8

Designation	Section	Steel grade	Number of bolts, n	Bolt	e_1 [mm]	e_2 [mm]	p_1 [mm]	$N_{ult,FEA}$ [kN]	U_{eff}	Failure mode
A8.1	$L60 \times 5$	S235	1	M18	70	26	–	62.1	0.36	–
A1.10	$L60 \times 5$	S275	1	M18	70	26	–	73.9	0.36	–
A8.2	$L60 \times 5$	S450	1	M18	70	26	–	94.9	0.36	–
A8.3	$L60 \times 5$	S235	2	M20	70	26	55	91.3	0.54	BT-L
A1.5	$L60 \times 5$	S275	2	M20	70	26	55	109.4	0.55	BT-L
A8.4	$L60 \times 5$	S450	2	M20	70	26	55	141.8	0.55	BT-L
A8.5	$L80 \times 5$	S235	3	M20	70	41	70	181.1	0.74	BT
A2.6	$L80 \times 5$	S275	3	M20	70	41	70	215.4	0.75	BT
A8.6	$L80 \times 5$	S450	3	M20	70	41	70	261.6	0.70	NT
A8.7	$L80 \times 5$	S235	3	M20	70	41	95	194.2	0.80	NT
A2.7	$L80 \times 5$	S275	3	M20	70	41	95	232.1	0.81	NT
A8.8	$L80 \times 5$	S450	3	M20	70	41	95	279.0	0.75	NT

Only in one element (A8.6) was a change in failure mode observed, from block tearing to net section tearing, according to the use of a higher grade of steel. There was also a slight decrease in the efficiency coefficient U_{eff} in elements connected with 3 bolts, in the case of steel S450 usage. Therefore, the influence of the steel grade in the range S235 ÷ S450 seems to be negligible on the failure mechanism.

4.6. The dependence of failure mode and geometrical parameters

Investigated damage evolution of angles connected by one leg shows both fracture along $A_{nt,1}$ zone and yielding of other parts (bands) of joints. Apart from typical and well-known failure modes, such as net tearing (fracture in one perpendicular section) and block tearing (fracture along the line of bolt holes on the tension face and plastic shear failure at the only one line of bolts), it was also observed an additional failure mode – limited block tearing.

In this failure mode, the failing block is surrounded from one side by rupture line, and from two others by yield lines (bands), Fig. 7. This failure mode has not been dealt with so far in design provisions, but appears to be similar to block tearing failure occurred under eccentric loading [25, 26]. Its appearance at angles connected by a one leg, by single row of bolts, depends on the ratio of e_1/e_2 (see Fig. 11, that presents the results of the entire range of carried out research). When the dimension e_1 exceeds about twice the dimension e_2 (the threshold value e_1/e_2 from the simulations lies between 1.71÷1.89), limited block tearing failure becomes dominant.
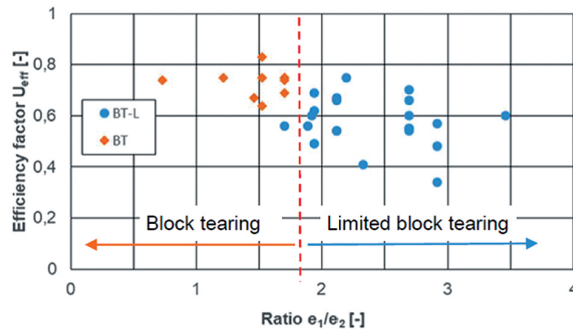
Fig. 11. Influence of the ratio e_1/e_2 on the failure mode

Net tearing of the cross section perpendicular to the direction of load transfer occurs in connections where the distance L_p between the centres of the end bolts in a joint, measured in the direction of force transfer, was greater than $5d_0$. Net tearing, as the only failure mode, occurs when the relative connection length $L_p/d_0 > 8$.

5. Conclusions

In this study, the ultimate net section resistance of angles connected by one leg was investigated using finite element models. The modelling was validated in the own experimental studies. The wide parametric analysis provided data on the emerging failure modes and the load-bearing capacity obtained from the net cross section.

Based on the results obtained, the following conclusions can be drawn:
– The Gurson–Tvergaard–Needleman material model, calibrated for structural steel, can be beneficial in understanding the real behaviour of connections and joints in which resistance is based on rupture.

– The resistance of the net section of angles connected by one leg is based on the mechanism of net tearing, block tearing and limited block tearing.
– Limited block tearing is a failure mode resulting from eccentricity of loading and depends on the e_1/e_2 ratio.

References

[1] G.L Kulak, E.Y. Wu, "Shear Lag in Bolted Angle Tension Members", *Journal of Structural Engineering*, 1997, vol. 123, no. 9, pp. 1144–1152; DOI: 10.1061/(asce)0733-9445(1997)123:9(1144).

[2] P. Može, "Angles connected by one leg in tension", *Ce/Papers*, 2017, vol. 1, no. 2-3, pp. 3771–3780; DOI: 10.1002/cepa.433.

[3] B. Jiang, M.C.H. Yam, K. Ke, A.C.C Lam, Q. Zhao, "Block shear failure of S275 and S690 steel angles with single-line bolted connections", *Journal of Constructional Steel Research*, 2020, vol. 170; DOI: 10.1016/j.jcsr.2020.106068.

[4] P. Može, "Statistical evaluation of bearing resistance and related strength functions for bolted connections", *Journal of Constructional Steel Research*, 2020, vol. 171, art. ID 106128; DOI: 10.1016/j.jcsr.2020.106128.

[5] W. Barcewicz, S. Wierzbicki, M.A. Giżejowski, S. Labocha, R. Czyż, "Experimental investigation of angle length effect – angles in tension connected by one leg", in *Modern trends in research on steel aluminium and composite structures*, M. Gizejowski, et al., Eds. 2021, pp. 85–91; DOI: 10.1201/9781003132134-7.

[6] C. Topkaya, "A finite element parametric study on block shear failure of steel tension members", *Journal of Constructional Steel Research*, 2004, vol. 60, no. 11, pp. 1615–1635; DOI: 10.1016/j.jcsr.2004.03.006.

[7] E.L. Salih, L. Gardner, D.A. Nethercot, "Numerical investigation of net section failure in stainless steel bolted connections", *Journal of Constructional Steel Research*, 2010, vol. 66, no. 12, pp. 1455–1466; DOI: 10.1016/j.jcsr.2010.05.012.

[8] R. Yan, H. Xin, M. Veljkovic, "Ductile fracture simulation of cold-formed high strength steel using GTN damage model", *Journal of Constructional Steel Research*, 2021, vol. 184, art. ID 106832; DOI: 10.1016/j.jcsr.2021.106832.

[9] A. Kanvinde, "Predicting Fracture in Civil Engineering Steel Structures: State of the Art", *Journal of Structural Engineering*, 2017, vol. 143, no. 3, art. ID 03116001; DOI: 10.1061/(asce)st.1943-541x.0001704.

[10] H. Wen, H. Mahmoud, "Simulation of block shear fracture in bolted connections", *Journal of Constructional Steel Research*, 2017, vol. 134, pp. 1–16; DOI: 10.1016/j.jcsr.2017.03.006.

[11] K. Ke, Y.H. Xiong, M.C.H. Yam, A.C.C.Lam, K.F. Chung, "Shear lag effect on ultimate tensile capacity of high strength steel angles", *Journal of Constructional Steel Research*, 2018, vol. 145, pp. 300–314; DOI: 10.1016/j.jcsr.2018.02.015.

[12] A.L. Gurson, "Continuum theory of ductile rupture by void nucleation and growth", *Journal of Engineering Materials and Technology*, 1977, vol. 99, no. 76, pp. 2–15.

[13] A. Needleman, V. Tvergaard, "An analysis of ductile rupture in notched bars", *Journal of the Mechanics and Physics of Solids*, 1984, vol. 32, no. 6, pp. 461–490; DOI: 10.1016/0022-5096(84)90031-0.

[14] X.D. Qian, Y.S. Choo, JYR. Liew, J. Wardenier, "Simulation of Ductile Fracture of Circular Hollow Section Joints Using the Gurson Model", *Journal of Structural Engineering*, 2005, vol. 131, no. 5, pp. 768–780; DOI: 10.1061/(ASCE)0733-9445(2005)131:5(768).

[15] F. Yang, M. Veljkovic, Y. Liu, "Ductile damage model calibration for high-strength structural steels", *Construction and Building Materials*, 2020, vol. 263, art. ID 120632; DOI: 10.1016/j.conbuildmat.2020.120632.

[16] E. Bernatowska, L. Ślęczka, "Numerical study of block tearing failure in steel angles connected by one leg", *Archives of Civil Engineering*, 2021, vol. 67, no. 1, pp. 269–283; DOI: 10.24425/ace.2021.136473.

[17] T. Soo Kim, H. Kuwamura, "Finite element modeling of bolted connections in thin-walled stainless steel plates under static shear", *Thin-Walled Structures*, 2007, vol. 45, no. 4, pp. 407–421; DOI: 10.1016/j.tws.2007.03.006.

[18] J. Kim, J.C. Yoon, B.S. Kang, "Finite element analysis and modeling of structure with bolted joints", *Applied Mathematical Modelling*, 2007, vol. 31, no. 5, pp. 895–911; DOI: 10.1016/j.apm.2006.03.020.

[19] E. Bernatowska, L. Ślęczka, "Experimental and numerical investigation into failure modes of tension angle members connected by one leg", *Materials*, 2021, vol. 14, no. 18; DOI: 10.3390/ma14185141.

[20] *EN 10025-1 Hot rolled products of structural steels – Part 1: General technical delivery conditions*. CEN, Brussels, 2007.

[21] P.G. Kossakowski, "Experimental determination of the void volume fraction for S235JR steel at failure in the range of high stress triaxialities", *Archives of Metallurgy and Materials*, 2017, vol. 62, no. 1, pp. 167–172; DOI: 10.1515/amm-2017-0023.

[22] P.G. Kossakowski, "Analysis of the void volume fractions for 235JR steel at failure for low initial stress triaxiality", *Archives of Civil Engineering*, 2018, vol. 64, no. 1, pp. 101–115; DOI: 10.2478/ace-2018-0007.

[23] E. Bernatowska, L. Ślęczka, "Net section fracture assessment of steel bolted joints with shear lag effect", *MATEC Web of Conferences*, 2019, vol. 262, art. ID 09002; DOI: 10.1051/matecconf/201926209002.

[24] E. Bernatowska, "Numerical simulations of ductile fracture in steel angle tension members connected with bolts", *Civil and Environmental Engineering Reports*, 2020, vol. 30, no. 2, pp. 32–54; DOI: 10.2478/ceer-2020-0018.

[25] J. Jönsson, "Block failure in connections -including effects of eccentric loads", in *Proc. 7th European Conference on Steel and Composite Structures (Eurosteel 2014), Napoli, Italy*, 10–12 Sept. 2014.

[26] S. Maleki, M. Ghaderi-Garekani, "Block shear failure in welded gusset plates under combined loading", *Journal of Constructional Steel Research*, 2020, vol. 170, art. ID 106079; DOI: 10.1016/j.jcsr.2020.106079.

Nośność przekroju osłabionego w kątownikach mocowanych jednym ramieniem

Słowa kluczowe: śrubowe połączenia zakładkowe, kątowniki stalowe, nośność graniczna na rozerwanie, rozerwanie blokowe, symulacje numeryczne

Streszczenie:

W stalowych konstrukcjach budowlanych kątowniki są stosowane najczęściej jako elementy rozciągane, głównie ze względu na łatwość ich wytwarzania i montażu. Ze względów praktycznych łączy się je tylko jednym ramieniem, za pomocą pojedynczego rzędu śrub, a zerwanie osłabionego przekroju decyduje zwykle o nośności całego połączenia. Na rozkład naprężenia w złączu i tym samym nośność przekroju netto wywiera również wpływ mimośród obciążenia.

Przy projektowaniu takich elementów, oprócz uwzględnienia nośności plastycznej przekroju brutto, należy wziąć pod uwagę nośność graniczną przekroju poprzecznego netto oraz nośność na rozerwanie blokowe. W obu tych ostatnich formach zniszczenia stanem granicznym jest rozerwanie materiału i ważne jest uwzględnienie opisu ciągliwego pękania stali w celu uzyskania miarodajnego oszacowania nośności. Wymaga to zaawansowanego modelowania materiału w porównaniu do dobrze już rozpoznanych zjawisk nośności plastycznej. W pracy przedstawiono symulację numeryczną zniszczenia przekroju netto połączenia kątowników rozciąganych, wykonanych ze stali konstrukcyjnej gatunku S275, z uwzględnieniem inicjacji i ciągliwej propagacji pęknięcia. Zastosowano model materiału Gursona–Tvergaarda–Needlemana. Przeprowadzono obszerną analizę parametryczną nośności granicznej i powstającej formy zniszczenia. Badano wpływ:

– stosunku szerokości ramienia do jego grubości b/t w kątownikach równoramiennych,

– rozstawu otworów na śruby w kierunku działania obciążenia p_1 i całkowitej długości połączenia L_p,

– odległości osi otworu od krawędzi w kierunku prostopadłym do kierunku działającego obciążenia e_2,

– odległości osi skrajnego otworu od krawędzi w kierunku równoległym do działającego obciążenia e_1, oraz

– zróżnicowania parametrów mechanicznych stali.

Zaobserwowano typowe, i dobrze już rozpoznane, mechanizmy zniszczenia takie, jak rozerwanie przekroju poprzecznego netto oraz rozerwanie blokowe. Analizy pokazały także dodatkową formę zniszczenia sklasyfikowaną jako ograniczone rozerwanie blokowego, która nie była dotychczas uwzględniana w przepisach projektowania. W artykule stwierdzono, że model materiału Gursona–Tvergaarda–Needlemana może być bardzo korzystny z punktu widzenia modelowania węzłów i połączeń, których nośność opiera się na rozerwaniu materiału. Przedstawiono także wpływ parametrów geometrycznych na powstające formy zniszczenia, w szczególności na nowo zaobserwowany mechanizm ograniczonego rozerwania blokowego.